IN-PLANE NONLINEAR STABILITY ANALYSIS OF SHALLOW ARCHES WITH ELASTIC SUPPORTS

by

Mengzhe Gu

Bachelor of Engineering, Southeast University, 2011

Submitted to the Graduate Faculty of

Swanson School of Engineering in partial fulfillment

of the requirements for the degree of

Master of Science

University of Pittsburgh

2013

UNIVERSITY OF PITTSBURGH

SWANSON SCHOOL OF ENGINEERING

This thesis was presented

by

Mengzhe Gu

It was defended on

April 1st, 2013

and approved by

Kent A. Harries, Ph.D, Associate Professor, Department of Civil and Environmental Engineering

John C. Brigham, Ph.D, Assistant Professor, Department of Civil and Environmental Engineering

Thesis Advisor: M.A.M Torkamani, PhD, Associate Professor, Department of Civil and Environmental Engineering

IN-PLANE NONLINEAR STABILITY ANALYSIS OF SHALLOW ARCHES WITH ELASTIC SUPPORTS

Mengzhe Gu, M.S.

University of Pittsburgh, 2013

Classical buckling theory has been researched extensively to determine the in-plane buckling behavior of parabolic, circular and catenary arches. To simplify the analyses, several assumptions are made. However, these simplified assumptions are not valid for shallow arches under significant vertical load which are characterized by their high geometric non-linearity. Prebuckling displacements should be accounted for for accurate in-plane buckling analysis of shallow arches. In reality, the supports of arches are not necessarily pin- or fixed-connections. An arch may be supported by elastic foundations or other structural elements that provide elastic restraint at the supports. In this work, elastic foundations are represented by horizontal and rotational springs. These support restraints may have a significant influence on the in-plane buckling behavior.

In-plane non-linear stability analysis of shallow arches is performed in this thesis. Energy equations are derived by considering the total potential energy of the

arch structure. The vanishing of first variation of total potential energy characterizes the equilibrium state, while the second variation of total potential energy falling to zero represents the transition from a stable state to an unstable state, from which the critical condition may be obtained.

Finally, this thesis discusses the effects of horizontal and rotational restraints in calculation of in-plane buckling strength of shallow arches. Several examples are considered to illustrate the application of the theory, presented in this research for general practice.

TABLE OF CONTENTS

LIST OF TABLES

LIST OF FIGURES

NOMENCLATURE

A area of the arch cross section

b width of cross section

E modulus of elasticity

f rise of the arch

h depth of cross section

I_x moment of inertia about x axis

L span of the arch

k_θ stiffness of rotational springs

k_z stiffness of horizontal springs

N actual compression force

N^* actual compression force in the buckled configuration

p focal parameter

P arbitrary point

P_e critical load for prismatic arch

q external distributed load

$[R]$ rotation matrix

r_x radius of gyration

s length of the arch

S half the length in arch axis

U strain energy

v displacement in the horizontal direction

v_b vertical displacement during buckling

v_c displacement at the crown

w displacement in the horizontal direction

w_b horizontal displacement during buckling

α horizontal stiffness ratio

β_θ rotational stiffness ratio

γ simplification coefficient

ε longitudinal normal strain

ε_m membrane strain

ε_m^* membrane strain in the buckled configuration

ε_{mb} membrane strain during buckling

ε_b bending strain

$\delta\,\varepsilon_m$ first variation of membrane strain

θ axial force coefficient

λ modified slenderness ratio

μ stability parameter

Π total potential energy

Π^* potential energy at buckled configuration

$\delta\,\Pi$ first variation of total potential energy

$\delta\,\Pi^*$ first variation of potential energy at buckled configuration

ω dimensionless load

Ω potential energy of external load

ACKNOWLEDGEMENT

Foremost, I would like to express my sincere gratitude to my advisor Professor Torkamani, for his patience, motivation, enthusiasm, and immense knowledge. His guidance helped me in all the time of research and writing of this thesis.

Besides my advisor, I would like to thank the rest of my thesis committee: Professor Harries and Professor Brigham for their encouragement and insightful comments.

My sincere thanks also go to my former roommates. It is their generous help that makes me adjusted to the life in North-America.

Last but not the least, I would like to thank my parents for their hard working. Nothing would ever happen without their constant financial and moral support. Love you.

1.0 INTRODUCTION

Arches as structural components or systems are extensively used in civil infrastructure due to their geometry that resolves external forces into compressive stresses. It is a very useful structural form since it takes advantage of tension-weak materials such as stone, cast iron and concrete which are able to resist compressive rather than tension, shear, or torsional forces. However, the in-plane structural behavior becomes non-linear as the external load increases, and when external load reaches a limit, the arch may buckle in a snap-through or bifurcation mode from the primary equilibrium path to a secondary equilibrium path.

The in-plane buckling of parabolic or circular arches were studied by early researchers (Timoshenko and Gere 1961, Gjelsvik and Bodner 1962, Schreyer and Masur 1966, Simitses 1976). The author of these early investigations made several simplified assumptions for buckling analysis: first, the prebuckling behavior is assumed to be linear, so stress and strain resultants could be linearized; second, the effects of pre-buckling displacements are neglected; third, the effects of post-buckling deformations on the displacements and geometric stiffness are also disregarded. Classic buckling theory is often utilized to dertermine the elastic buckling load of arches (Timoshenko and Gere 1961, Simitses 1976), however, several simplifications have to be made as discussed in the Introduction.

Austin (1971) summerrizd the work presented by Timoshenko and Gere (1961) and the work of Dinnik (1955), and stuied the behavior of elastic buckling for fixed, two hinged and three hinged arches subject to unifrom load on horizontal

projection. He suggested that for prismatic arches under pure compression, the critical axial load can be expresed in an identical form to those used for straight compression members as

$$P_e = \eta \frac{EI}{S^2} = \pi^2 \frac{EI}{(kS)^2}$$

where P_e is the critical axial compressive force at the quarter points of the span; E is the Young's modulus; I is the moment of inertia; S is one half of the length of arch axis; k is the effective length factor; η is a coefficient. The parameters η and k are generated from the work of Timoshenko and Gere 1961 and Dinnik 1955, where buckling differential equations are assumed to be linear. This differential equation is characterized by the inextensionality of the centroidal axis and neglecting the squares and products of small increments in the displacement which is small enough. The values of η and k given by Austin (1971) are listed in the Table 1.

Table 1. Values of η and k in classic buckling theory

$\frac{f}{L}$	Pin-ended Arch		Fixed Arch	
	η	k	η	k
0.1	9.56	1.02	20.4	0.7
0.2	9.21	1.04	20.5	0.69
0.3	8.19	1.10	20.3	0.7
0.4	7.81	1.12	19.7	0.71
0.5	7.42	1.15	18.8	0.72

The following obervations can be made: first, the critical load at quarter points is a function of the arch types and and arch rise–span ratio; second, the effective length factor for arches are extremely similar to the straight column with the same support conditions, i.e. 0.65 for fixed column and 1.00 for pin-pin column.
However, these simplifications in classical buckling theory are not valid for shallow arches under significant vertical load. In-plane displacements of these arches are large and non-linear, therefore, the prebuckling displacements should be accounted for in the calculation of the buckling load.

Timoshenko and Gere (1961) and Gjelsvik and Bodner (1962) obtained approximate solutions for various shallow arch buckling problems. Schreyer and Masur (1966) performed an analytical study for shallow circular arches subject to radial pressure, however, the analysis was limited to fixed supports and a rectangular solid section and they may not represent reality. Dickie and Broughton (1971) used a series method to study shallow circular pin-ended and fixed arches subjected to a central concentrated load, a radial pressure, or a linearly varying radial load. Reasonable numerical solutions are given; however, their study was also confined again to rectangular solid cross sections. Power and Kyriakides (1994) studied the behavior of long shallow elastic panels under uniform pressure loading and demonstrated that shallow arches are characterized by nonlinearity and instability. In addition to rectangular sections, other shapes such as I-section, hollow-sections are extensively used for arches.

More recently, Pi et al. (2002) investigated in-plane buckling behavior of fixed and pin-ended shallow circular arches with arbitrary cross sections that are subject to uniform radial load around the arch axis; they obtained the close form solutions for their cases. Bradford et al. (2002) generated the analytical solution for a central concentrated load with fixed and pin-ended support. Bradford, Pi and Gilbert

(2004) extended the previous study and investigated the limit of modified slenderness ratio which determines the threshold of symmetric and anti-symmetric buckling.

The considerable compression force in the shallow arch leads to high reaction forces at the supports. In a typical engineering structure where supports are embedded in bedrock or on piles of stiff concrete, some relative horizontal and rotational movements due to the high reaction forces is expected. Therefore, the supports of a shallow arch may realistically be modeled with combinations of horizontal and rotational springs, as shown in Figure 1.

There is plenty of research papers on the topic of stability analysis of shallow arches, however, those authors only considered arches to be supported by ideal conditions, such as pin, fixed or lateral restraint support. The motivation of this thesis research is to have a better understanding of stability of shallow arches which are supported by both horizontal and rotational restraints.

The purpose of this thesis is to extend the work of Bradford, Pi and Gilbert (2004) to the investigation of the in-plane buckling of shallow parabolic arches under uniform distributed load, with supports that are modeled with horizontal and rotational springs. The variation of total potential energy is used to establish the nonlinear equilibrium equations and to obtain analytical solutions of the buckling loads for both symmetric and anti-symmetric buckling modes.

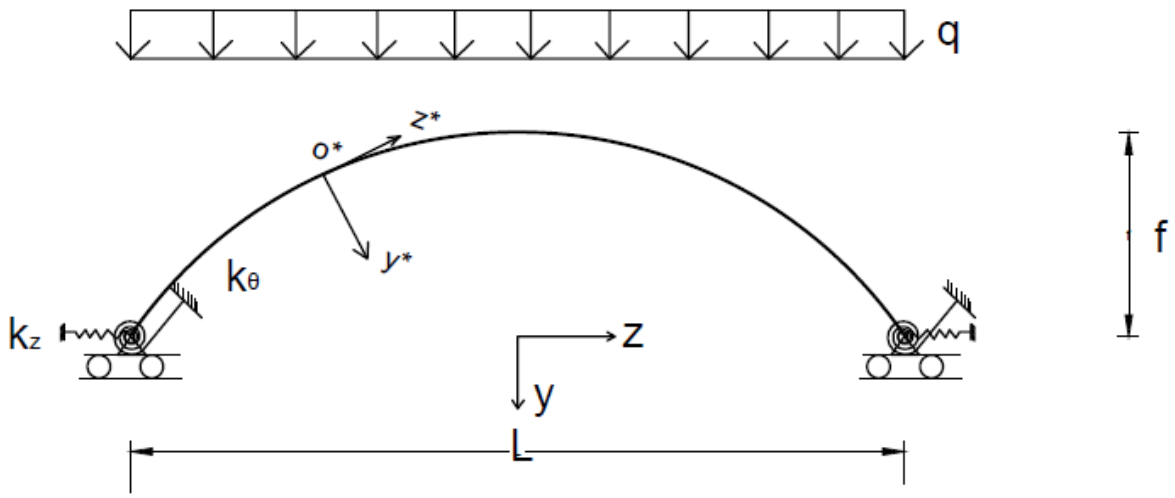

Figure 1. Geometry and loading of the parabolic arch

2.0 DIFFERENTIAL EQUILIBRIUM EQUATIONS

The parabolic arch shown in Figure 1 is subjected to a vertical uniformly distributed load q per unit length. A fixed coordinate system yz is defined to describe the geometry and the deformation of the arch, as shown in Figure. 1. The origin of the axis system is at the center between the two supports of the arch, with the positive direction of the axis y being vertically downward and the positive direction of the axis z being toward the right end of the arch. With this axis system, the profile of the parabolic arch centerline can be expressed as

$$y = \frac{1}{2p}[z^2 - (\frac{L}{2})^2] \qquad z \in [\frac{-L}{2} \ , \ \frac{L}{2}] \tag{1}$$

where L is the span of the arch, and the focal parameter p of the parabola is defined by (Bradford et al. 2004)

$$p = \frac{L^2}{8f} \tag{2}$$

where f is the rise of the arch.

An axes system y^*z^* is also defined in Figure 1, where the axis z^* runs around the arch, tangent to the locus of the centroids of the arch cross sections and the axis y^* corresponds to the centroidal axis of each cross section in the plane of the arch perpendicular to the z^* axis.

The arch is supported vertically by rollers, and has horizontal and rotational springs with stiffness of k_z and k_θ, respectively, as shown in Figure 1. Vertical displacements at the supports of the arch are fully restrained by the rigid foundation.

In this study, the stiffness of the two pairs horizontal springs and rotational springs of an arch are assumed to be equal to each other, so that the arch is supported symmetrically.

The basic assumptions used in this thesis are: (1) the arch, its elastic springs at the supports, and the vertical load form a conservative system, so that energy methods may be used in the investigation; (2) the arches are assumed to be shallow so that

$(dy/dz)^2 << 1$, and thus $ds = dz\sqrt{1+(\frac{dy}{dz})^2} \cong dz$; (3) the material from which the arch is fabricated is linear elastic.

After deformation, the origin o^* moves to O^*, and axes system y^*z^* rotates to a new position Y^*Z^*.

The rotation matrix which describe the relationship between axes coordinates $o^*y^*z^*$ and $O^*Y^*Z^*$ are shown as following

$$R = \begin{bmatrix} 1 & \frac{dv^*}{ds} \\ -\frac{dv^*}{ds} & 1 \end{bmatrix} \tag{3}$$

where v^* is the normal displacement in the y^* direction, and *ds* is the small increment of the arch length, tangent to the arch centerline. As shown in Figure 2.

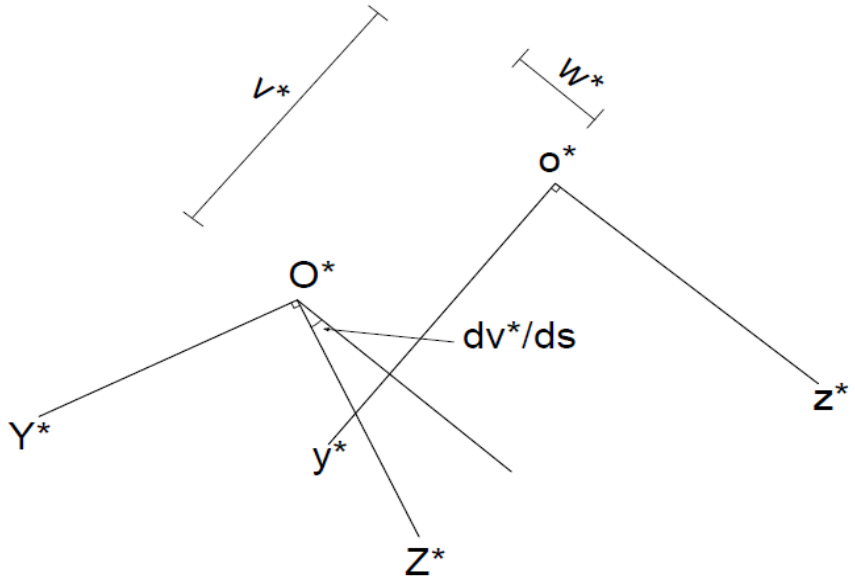

Figure 2. Axes and rotations of parabolic arch

The relation between normal displacement v^* in the y^*-direction and v in the y-direction may be expressed as

$$v = v^* \cos\theta \tag{4}$$

where θ is the angle between moving axis y^* and fixed axis y.

According to the previous basic assumptions, it can be shown $\frac{dv^*}{ds} = \frac{dv}{dz}$, and therefore, the rotation matrix may be rewritten as (Torkmani 1998)

$$R = \begin{bmatrix} 1 & v' \\ -v' & 1 \end{bmatrix} \tag{5}$$

in which $()' \equiv d()/dz$.

An arbitrary point $P(x^*, y^*, 0)$ on the cross section of the arch after deformation moves to $P'(x^*, y^* + v^*, w^*)$. Therefore, the displacements of an arbitrary point P in

y- and *z* -directions may be expressed in term of centroidal displacements by Eq. (6) (Torkamani et al. 2009).

$$\begin{Bmatrix} v_p \\ w_p \end{Bmatrix} = \begin{Bmatrix} v \\ w \end{Bmatrix} + R\begin{Bmatrix} y^* \\ 0 \end{Bmatrix} - \begin{Bmatrix} y^* \\ 0 \end{Bmatrix} \tag{6}$$

The first term on the right hand side of Eq. (6) represents the translation of point P, and the second and third terms represent the rotation of point P.

Substituting rotation matrix, Eq. (5) into Eq. (6) gives

$$\begin{Bmatrix} v_p \\ w_p \end{Bmatrix} = \begin{Bmatrix} v \\ w - y^* v' \end{Bmatrix} \tag{7}$$

The longitudinal normal strain ε may be obtained using Lagrangian strain expression

$$\varepsilon = \frac{1}{2}\frac{(ds^*)^2 - (ds)^2}{(ds)^2} \tag{8}$$

where ds and ds^* are the length of infinitesimal element at point P before and after the deformation

$$(ds)^2 = (dy)^2 + (dz)^2 \tag{9}$$

and

$$(ds^*)^2 = (dy + dv_p)^2 + (dz + dw_p)^2 \tag{10}$$

Substituting for v_p and w_p from Eq. (7) into Eq. (10) yields

$$(ds^*)^2 = (dy + dv)^2 + (dz + dw - y^* dv')^2 \tag{11}$$

Substituting Eqs. (9) and (11) into Eq. (8), using assumption $(dy/dz)^2 << 1$ and neglecting higher order terms $\frac{1}{2}(w')^2, \frac{1}{2}(y^* v'')^2, (-y^* w' v'')$, produces, the non-linear strain-displacement relationships on the cross section for point P

$$\varepsilon = w' + \frac{v'z}{p} + \frac{1}{2}(v')^2 - y^* v'' \tag{12}$$

where the total strain consist of membrane and bending strain which are given by

$$\varepsilon = \varepsilon_m + \varepsilon_b \tag{13}$$

where

$$\varepsilon_m = w' + \frac{v'z}{p} + \frac{1}{2}(v')^2 \tag{14}$$

and

$$\varepsilon_b = -y^* v'' \tag{15}$$

w and v are displacements in the z and y directions, respectively. The term $\frac{1}{2}(v')^2$ is the source of the geometric nonlinearity.

A variational method based on the first variation of total potential energy is used here to investigate the in-plane elastic buckling of shallow arches by considering the effects of the prebuckling deformations and geometric nonlinearity, which classical buckling theory does not account for. The total potential energy Π of a shallow arch subject to uniform distributed load with elastic supports may be written as

$$\Pi = U + \Omega \tag{16}$$

in which strain energy U and potential energy of external forces Ω are expressed as following

$$U = \frac{1}{2}\int_{VOL} E\varepsilon^2 dvol + \sum_{i=\pm L/2} \frac{1}{2} k_z w_i^{\,2} + \sum_{i=\pm L/2} \frac{1}{2} k_\theta (v_i')^2 \text{ and } \quad \Omega = -\int_{-L/2}^{L/2} qv dz \tag{17}$$

The nonlinear in-plane equilibrium equations for the arch can be derived from the first variation of total potential energy, which requires

$$\delta\Pi = \int_{VOL} E\varepsilon\delta\varepsilon \, dvol - \int_{-L/2}^{L/2} q\delta v dz + \sum_{i=\pm L/2} k_z w_i \delta w_i + \sum_{i=\pm L/2} k_\theta v_i' \delta v_i' = 0 \tag{18}$$

For an arch with a constant cross section

$$dvol = A\, ds \tag{19}$$

Based on the assumption that $ds \cong dz$, Eq. (19) can be rewritten as

$$dvol = A\,dz \tag{20}$$

Using Eq. (20), and substituting Eq. (12) into Eq. (18), leads to

$$\delta\Pi = \int_{-L/2}^{L/2} (EA\varepsilon_m \delta\varepsilon_m + EI_x v''\delta v'' - q\delta v)dz + \sum_{i=\pm L/2} k_z w_i \delta w_i + \sum_{i=\pm L/2} k_\theta v_i' \delta v_i' = 0 \tag{21}$$

where

$$\delta\varepsilon_m = \delta w' + \frac{z\delta v'}{p} + v'\delta v'.$$

The first variation of total potential energy, Eq. (21), contains two parts

$$\int_{-L/2}^{L/2} EA\varepsilon_m \delta w' dz + \sum_{i=\pm L/2} k_z w_i \delta w_i = 0 \tag{22}$$

and

$$\int_{-L/2}^{L/2} [EA\frac{z}{p}\varepsilon_m \delta v' + EA\varepsilon_m v'\delta v' + EI_x v''\delta v'' - q\delta v]dz + \sum_{i=\pm L/2} k_\theta v_i' \delta v_i' = 0 \tag{23}$$

for the horizontal and vertical directions, respectively.

Consider Eq. (22) and integrate by part leads to

$$EA\varepsilon_m \delta w\Big|_{-L/2}^{L/2} - \int_{-L/2}^{L/2} \frac{d}{dz}(EA\varepsilon_m)\delta w dz + \sum_{i=\pm L/2} k_z w_i \delta w_i = 0 \tag{24}$$

Since δw is a virtual displacement that varies arbitrarily, therefore, is not equal to zero, $\frac{d}{dz}(EA\varepsilon_m) = 0$, for constant EA

$$EA\varepsilon_m' = 0 \tag{25}$$

Therefore, $EA\varepsilon_m$ is constant and the boundary conditions are obtained from Eq. (24) as

$$EA\varepsilon_m + k_z w_{L/2} = 0 \tag{26}$$

$$EA\varepsilon_m - k_z w_{-L/2} = 0 \tag{27}$$

Consider Eq. (23) and integrate by part gives:

$$EA\varepsilon_m \frac{z}{p}\delta v\Big|_{-L/2}^{L/2} - \int_{-L/2}^{L/2} \frac{EA\varepsilon_m}{p} dz\delta v + EA\varepsilon_m v'\delta v\Big|_{-L/2}^{L/2} - \int_{-L/2}^{L/2} EA\varepsilon_m v''dz\delta v + EI_x v''\delta v'\Big|_{-L/2}^{L/2} - EI_x v'''\delta v\Big|_{-L/2}^{L/2} + \int_{-L/2}^{L/2} EI_x v^{\mathrm{IV}} dz\delta v + \sum_{i=\pm L/2} k_\theta v_i'\delta v_i' = 0 \tag{28}$$

For all sets of kinematically admissible virtual displacements δv, Eq. (28) leads to

$$EI_x v^{IV} - \frac{EA}{p}\varepsilon_m - EA\varepsilon_m v'' - q = 0 \tag{29}$$

And the boundary conditions are also obtained as

$$(EI_x v'' + k_\theta v')_{L/2} = 0 \tag{30}$$

$$(EI_x v'' - k_\theta v')_{-L/2} = 0 \tag{31}$$

From Eq. (25), the membrane strain ε_m is known to be constant and can be rewritten as

$$-\varepsilon_m = \frac{N}{EA} \tag{32}$$

where N is the actual compression force in the arch. Introducing the stability parameter μ and the dimensionless load ω defined by

$$\mu = \sqrt{\frac{N}{EI_x}} \tag{33}$$

and

$$\omega = \frac{qp - N}{N} \tag{34}$$

then substituting Eq. (32) to (34) into Eq. (29) leads to the differential equilibrium equation for the vertical displacement as

$$v^{IV} + \mu^2 v'' = \frac{\mu^2 \omega}{p} \tag{35}$$

3.0 NON-LINEAR EQUATION OF EQUILIBRIUM

The vertical displacement v can be calculated from the solution of Eq. (35). The geometric boundary conditions are $v=0$ at $z=\pm\frac{L}{2}$ and force boundary conditions are given by Eqs. (30) and (31).

Integrate Eq. (35) twice gives

$$v''+\mu^2 v=\frac{\omega\mu^2}{2p}z^2+E_1 z+E_2 \tag{36}$$

The solution to this second order differential equation is the sum of a homogenous and particular solution in the following form

$$v_{\mathrm{H}}=A\cos(\mu z)+B\sin(\mu z) \tag{37}$$

$$v_{\mathrm{P}}=E_3 z^2+E_4 z+E_5 \tag{38}$$

Substitute v_p and (v_p'') into Eq. (36) gives the coefficients E_3, E_4 and E_5 in terms of E_1 and E_2.

Therefore, the general solution to Eq. (35) becomes

$$v=A\cos(\mu z)+B\sin(\mu z)+\frac{\omega}{2p}z^2+\frac{E_1}{\mu^2}z+\frac{1}{\mu^2}(E_2-\frac{\omega}{p}) \tag{39}$$

Coefficients A, B, E_1 and E_2 in Eq. (39) are calculated using boundary conditions $v=0$ at $z=\pm\frac{L}{2}$ and Eqs. (30) to (31).

Applying $v=0$ at $z=\pm\frac{L}{2}$ to Eq. (33) gives

$$A\cos(\frac{\mu L}{2})+B\sin(\frac{\mu L}{2})+\frac{wL^2}{8p}+\frac{E_1 L}{2\mu^2}+\frac{1}{\mu^2}(E_2-\frac{w}{p})=0 \tag{40}$$

and

$$A\cos(\frac{\mu L}{2}) - B\sin(\frac{\mu L}{2}) + \frac{wL^2}{8p} - \frac{E_1 L}{2\mu^2} + \frac{1}{\mu^2}(E_2 - \frac{w}{p}) = 0 \tag{41}$$

Similarly, applying boundary conditions of Eqs. (30) and (31) gives

$$EI_x(-\mu^2 A\cos\theta - \mu^2 B\sin\theta + \frac{w}{p}) + k_\theta(-\mu A\sin\theta + \mu B\cos\theta + \frac{wL}{2p} + \frac{E_1}{\mu^2}) = 0 \tag{42}$$

and

$$EI_x(-\mu^2 A\cos\theta + \mu^2 B\sin\theta + \frac{w}{p}) + k_\theta(-\mu A\sin\theta - \mu B\cos\theta + \frac{wL}{2p} - \frac{E_1}{\mu^2}) = 0 \tag{43}$$

Solving Eqs. (40) to (43) together gives the coefficients as following

$$A = \frac{\gamma\,\omega}{\mu^2 p\cos(\theta)} \tag{44}$$

$$B = 0 \tag{45}$$

$$E_1 = 0 \tag{46}$$

$$E_2 = \frac{\omega}{p}(1 - \gamma - \frac{\theta^2}{2}) \tag{47}$$

Therefore, Eq. (39) becomes:

$$v = \frac{\gamma\omega[\cos(\mu z) - \cos\theta]}{\mu^2 p\cos\theta} + \frac{\omega(\mu^2 z^2 - \theta^2)}{2\mu^2 p} \tag{48}$$

where $\theta = \frac{\mu L}{2}$ (49)

is the axial force coefficient (Cai et al. 2010) and the coefficient γ is defined as

$$\gamma = \frac{\beta_\theta + 2}{2 + \beta_\theta \frac{\tan\theta}{\theta}} \tag{50}$$

and

$$\beta_\theta = \frac{k_\theta L}{EI_x} \tag{51}$$

is the stiffness ratio of the rotational spring and the arch.

Because the ends of the arch are support by horizontal springs, $\delta w_{-L/2} \neq 0$ and $\delta w_{L/2} \neq 0$. Hence, from Eq. (26) and (27), horizontal displacement at $z = \pm L/2$ can be obtained as

$$w_{-L/2} = \frac{EA\varepsilon_m}{k_z} \quad \text{and} \quad w_{L/2} = \frac{-EA\varepsilon_m}{k_z} \tag{52}$$

Substituting Eqs. (32), (33), and (49) into Eq. (52), the horizontal displacement at the support may be rewritten as

$$w_{-L/2} = \frac{-4\theta^2 EI_x}{k_z L^2} \quad \text{and} \quad w_{L/2} = \frac{4\theta^2 EI_x}{k_z L^2} \tag{53}$$

The nonlinear equilibrium conditions for shallow arches may be derived by reasoning that the constant membrane strain given by Eq. (32) is equal to the average membrane strain over the arch span L calculated from Eq. (14)

$$-\frac{N}{EA} = \frac{1}{L}\int_{-L/2}^{L/2} [w' + \frac{v'z}{p} + \frac{1}{2}(v')^2]\, dz \tag{54}$$

Considering Eq. (33), the left side of Eq. (54) may be rewritten as

$$-\frac{N}{EA} = -\frac{N}{EI_x}\frac{I_x}{A} = -\mu^2 r_x{}^2 \tag{55}$$

where r_x is the radius of gyration of the cross section about the major principal x-axis given by

$$r_x = \sqrt{\frac{I_x}{A}} \tag{56}$$

Considering Eq. (53) and substituting Eqs. (48) and (55) into Eq. (54), leads to the nonlinear equilibrium condition for a shallow parabolic elastic arch with horizontal spring supports, given by

$$A_1\omega^2 + B_1\omega + C_1 = 0 \tag{57}$$

where

$$A_1 = \frac{1}{4\theta^3}[4\theta\gamma - 4\gamma\tan\theta + \frac{2}{3}\theta^3 + \theta\gamma^2 + \theta\gamma^2\tan^2\theta - \gamma^2\tan\theta] \quad (58)$$

$$B_1 = \frac{1}{\theta^2}[\gamma - \frac{\gamma\tan\theta}{\theta} + \frac{\theta^2}{3}] \quad (59)$$

$$C_1 = (\frac{\theta}{\lambda})^2[1 + \frac{EA}{L}\frac{2}{k_z}] = (\frac{\theta}{\lambda})^2[1 + 2\alpha] \quad (60)$$

in which λ and α are the modified slenderness ratio and stiffness ratio, and they are defined as

$$\lambda = \frac{L^2}{4r_x p} = 2(\frac{f}{r_x}) \quad (61)$$

$$\alpha = \frac{EA}{Lk_z} \quad (62)$$

For an arch supported by pin and rotational springs only, k_z becomes infinite and α equals to zero, A_1 and B_1 remain the same given by Eqs. (58) and (59).

Coefficient C_1 changes to

$$C_1^* = (\frac{\theta}{\lambda})^2 \quad (60a)$$

The coefficients A_1, B_1 and C_1^* are consistent with those obtained by Cai (Cai J. et al. 2010) without considering the temperature gradient.

For a pin-supported arch, the stiffness k_z approaches infinity, while k_θ approaches zero, therefore, from Eqs. (50), (51) and (62), one may have

$$\beta_\theta = 0 \quad (63)$$

$$\gamma = 1 \quad (64)$$

$$\alpha = 0 \quad (65)$$

Then coefficients $A_1, B_1,$ and C_1 given by Eq. (58) to (60) reduce to

$$A_1^* = \frac{1}{4\theta^3}(5\theta - 5\tan\theta + \theta\tan^2\theta + \frac{2}{3}\theta^3) \tag{66}$$

$$B_1^* = \frac{1}{\theta^2}(1 - \frac{\tan\theta}{\theta} + \frac{\theta^2}{3}) \tag{67}$$

$$C_1^* = (\frac{\theta}{\lambda})^2 \tag{68}$$

which are the same as those obtained by Bradford (Bradford et al. 2004, 2007) for a pin-ended parabolic arch.

4.0 BUCKLING ANALYSIS

4.1 BUCKLING EQUATIONS

The arch may buckle from a prebuckled equilibrium configuration defined by (v, w) to a buckled equilibrium configuration defined by $(v^* = v + v_b, w^* = w + w_b)$, where v_b and w_b are the additional buckling displacements in the vertical and horizontal directions, respectively. The total potential energy at the buckled configuration is

$$\Pi^* = \frac{1}{2}\int_{VOL} E(\varepsilon^*)^2 dvol + \sum_{i=\pm L/2}\frac{1}{2}k_z(w_i^*)^2 + \sum_{i=\pm L/2}\frac{1}{2}k_\theta(v_i'^*)^2 - \int_{-L/2}^{L/2} qv^* dz \tag{69}$$

Consider $dvol = A\,dz$, the variation of total potential energy of Eq. (69) can be calculated as

$$\delta\Pi^* = \int_{-L/2}^{L/2}[EA\varepsilon_m^*\,\delta\varepsilon_m^* + EI_x(v^*)''(\delta v^*)'']dz - \int_{-L/2}^{L/2} q\delta v^* dz + + \sum_{i=\pm L/2} k_z(w_i^*)\delta w_i^* + \sum_{i=\pm L/2} k_\theta(v_i^*)'(\delta v_i^*)' \tag{70}$$

where $\varepsilon_m^* = (\delta w^*)' + \dfrac{(\delta v^*)'z}{p} + (v^*)'(\delta v^*)'$

In the buckled configuration, the first variation of total potential energy may also be used for equilibrium, which requires

$$\delta\Pi^* = \int_{-L/2}^{L/2}\{[EA(\delta w^*)' + (\delta v^*)'\frac{z}{p} + (v^*)'(\delta v^*)']\varepsilon_m^* + EI_x(v^*)''(\delta v^*)''\}dz - \int_{-L/2}^{L/2} q\delta v^* dz$$
$$+ \sum_{i=\pm L/2} k_z(w_i^*)\delta w_i^* + \sum_{i=\pm L/2} k_\theta(v_i^*)'(\delta v_i^*)' = 0 \tag{71}$$

Integrating Eq. (71) by parts leads to

$$EA\varepsilon_m^*\delta w^*\Big|_{-L/2}^{L/2} - \int_{-L/2}^{L/2}\frac{d}{dz}(EA\varepsilon_m^*)\delta w^* dz + \sum_{i=\pm L/2} k_z w_i^* \delta w_i^* = 0 \tag{72}$$

for the horizontal buckled deformation and

$$EI_x(v^*)^{IV} - \frac{EA}{p}\varepsilon_m^* - EA(v^*)''\varepsilon_m^* - q = 0 \tag{73}$$

for the vertical buckled deformation of the arch.

In Eq. (72), δw^* is a horizontal virtual displacement in the bucked configuration which is not equal to zero, $\frac{d}{dz}(EA\varepsilon_m^*) = 0$. For arch with uniform cross section, EA is constant and

$$EA(\varepsilon_m^*)' = 0 \tag{74}$$

Since $\delta w^*_{\pm L/2}$ and $\delta(v^*)'_{\pm L/2}$ have virtual values and are not equal to zero, the boundary conditions are obtained as

$$(EA\varepsilon_m^* + k_z w^*)_{L/2} = 0 \tag{75}$$

$$(EA\varepsilon_m^* - k_z w^*)_{-L/2} = 0 \tag{76}$$

for the horizontal direction and

$$[EI_x(v^*)'' + k_\theta (v^*)']_{L/2} = 0 \tag{77}$$

$$[EI_x(v^*)'' - k_\theta (v^*)']_{-L/2} = 0 \tag{78}$$

for the vertical direction.

From Eq. (74), the membrane strain in the buckled configuration is known to be a constant and can be written as

$$-\varepsilon_m{}^* = \frac{N^*}{EA} \tag{79}$$

where N^* is actual axial compressive force in the arch in the buckled configuration. Also in the buckled configuration

$$(\mu^*)^2 = \frac{N^*}{EI_x} \tag{80}$$

Subtracting Eq. (29) from Eq. (73) and considering

$$v^* = v + v_b \tag{83}$$

and the increment of membrane strain during buckling

$$\varepsilon_{mb} = \varepsilon_m^* - \varepsilon_m \tag{84}$$

gives

$$EI_x (v_b)^{IV} - EA\varepsilon_m^* (v_b)'' = EA\varepsilon_{mb} v'' + \frac{EA\varepsilon_{mb}}{p} \tag{85}$$

Eq. (85) may be rearranged in the following form

$$v_b{}^{IV} + (\mu^*)^2 v_b'' = \frac{\varepsilon_{mb}}{r_x{}^2}(v'' + \frac{1}{p}) \tag{86}$$

4.2 BIFURCATION BUCKLING

An arch that is subject to uniform distributed load may buckle in an anti-symmetric bifurcation mode. Bifurcation is an intermediate stage which is characterized by the fact that as the load passes the critical value, the arch passes from its prebuckled equilibrium configuration to an infinitesimally close buckled equilibrium configuration. Therefore, axial compressive force in the arch during bifurcation buckling is infinitesimally close to N , that is

$$N^* = N \tag{87}$$

The constant membrane $\varepsilon_m *$ given by Eq. (79) can then be written as

$$\varepsilon_m * = \frac{-N}{EA} \tag{88}$$

Thus

$$\mu^* = \mu$$

As a result, the membrane strain ε_{mb} during bifurcation buckling can be obtained by substituting Eqs. (32) and (88) into Eq.(84) as

$$\varepsilon_{mb} = \varepsilon_m{}^* - \varepsilon_m = \frac{-N}{EA} - \frac{-N}{EA} = 0 \tag{89}$$

Substituting $\varepsilon_{mb} = 0$ and $\mu^* = \mu$ into Eq. (86) leads to the differential equation for anti-symmetric bifurcation buckling given by

$$v_b{}^{IV} + \mu^2 v_b'' = 0 \tag{90}$$

Boundary conditions in bifurcation buckling can be obtained by subtracting Eqs. (77) and (78) from Eqs. (30) and (31)

$$[EI_x (v_b)'' + k_\theta (v_b)']_{L/2} = 0 \tag{91}$$

$$[EI_x (v_b)'' - k_\theta (v_b)']_{-L/2} = 0 \tag{92}$$

The general solution of Eq. (90) has the form

$$v_b = G_1 \cos(\mu z) + G_2 \sin(\mu z) + G_3 z + G_4 \tag{93}$$

Using the boundary condition $v_b = 0$ at $z = \pm L/2$ and Eqs. (91) and (92) leads to four linear homogenous algebraic equations with respect to G_1 to G_4.These four equations may be written in a matrix form as

$$\begin{bmatrix} C & S & L/2 & 1 \\ C & -S & -L/2 & 1 \\ -k_\theta \mu S - EI_x \mu^2 C & k_\theta \mu C - EI_x \mu^2 S & k_\theta & 0 \\ -k_\theta \mu C - EI_x \mu^2 S & -k_\theta \mu C + EI_x \mu^2 S & k_\theta & 0 \end{bmatrix} \begin{Bmatrix} G_1 \\ G_2 \\ G_3 \\ G_4 \end{Bmatrix} = \{0\} \tag{94}$$

where $S = \sin(\theta)$ and $C = \cos(\theta)$.

For the existence of non-trivial solutions for G_1 to G_4, the determinant of the coefficient matrix of the four linear algebraic equations must vanish, which yields

$$[\cos(\theta) + \frac{\beta_\theta \sin(\theta)}{2\theta}][\frac{\beta_\theta \sin(\theta)}{2} + \theta^2 (\sin\theta - \frac{\beta_\theta \cos(\theta)}{2\theta})] = 0 \tag{95}$$

For the sake of simplicity, assume the first term of Eq. (95) to be called $f(\theta)$ and the second term to be $g(\theta)$, thus

$$f(\theta) = \cos(\theta) + \frac{\beta_\theta \sin(\theta)}{2\theta} \tag{96}$$

and

$$g(\theta) = \frac{\beta_\theta \sin(\theta)}{2} + \theta^2 (\sin\theta - \frac{\beta_\theta \cos(\theta)}{2\theta}) \tag{97}$$

One may observe that $f(\theta)$ is an even function, $f(-\theta) = f(\theta)$, and $g(\theta)$ is an odd function, $g(-\theta) = -g(\theta)$.

When Eq. (96) is set to zero, the axial force coefficient $\theta = \theta_{sym}$, and the corresponding buckling shape is symmetric, which will not induce anti-symmetric bifurcation buckling. When Eq. (97) is set to zero, the coefficient $\theta = \theta_{ant}$, the corresponding buckling shape is anti-symmetric. Then the anti-symmetric buckling shape can be obtained by calculating coefficients G_1 to G_4. The value of G_1 to G_4 are

$$G_1 = G_4 = 0 \tag{98}$$

$$G_3 = \frac{-2G_2 \sin\theta}{L} \tag{99}$$

Substituting Eqs. (98) and (99) into v_b gives the anti-symmetric buckling shape as

$$v_{bant} = G_2[\sin(\mu z) - \frac{\mu z \sin(\theta)}{\theta}] \tag{100}$$

where G_2 is an amplifier parameter.

For anti-symmetric buckling, the solution of Eq. (97) may be expressed as

$$\tan(\theta) = \frac{\theta}{1 + \frac{2\theta^2}{\beta_\theta}} \tag{101}$$

from which the solution for θ is obtained

$$\theta_{ant} = n_{ant}\pi \tag{102}$$

where n_{ant} is a constant dependent on the value of β_θ.

Substitute Eq. (102) for θ in $\theta = \frac{\mu L}{2}$, and using Eq. (33), gives

$$N_{ant} = \frac{(n_{ant}\pi)^2 EI_x}{(L/2)^2} = N_E \tag{103}$$

where N_E is the second mode flexural buckling load of rotationally restraint pin-ended column.

It can be seen from the transcendental Eq. (101) that when supports are pin-ended ($\beta_\theta = 0$), the fundamental solution to $\tan\theta = 0$ is $\theta = \pi$. When supports are fixed ($\beta_\theta = \infty$), the fundamental solution to $\tan\theta = \theta$ is $\theta = 1.4303\pi$. Therefore, as rotational stiffness varies from zero to infinity, the corresponding n_{ant} obtained in Eq. (101) has the range of:

$$1 \le n_{ant} \le 1.4303 \tag{104}$$

The anti-symmetric buckling load $q_{ant}p$ may be obtained by solving Eq. (57). Note that $\omega = \frac{q_{ant}p}{N} - 1$

$$\frac{q_{ant}p}{N} = \frac{-B_1 \pm \sqrt{B_1^2 - 4A_1C_1}}{2A_1} + 1 \tag{105}$$

For pin-supported shallow arches, $\tan\theta = 0$, $\theta = \pi$ and $\gamma = 1$. If one substitute these data in Eqs. (58) to (60), the solution of Eq. (105) that indicates anti-symmetric buckling is real when $\lambda_{ant} \ge 7.83$. This result is consistent with that obtained by Bradford et al. (2004).

For a fix-supported shallow arches, the threshold of modified slenderness ratio for anti-symmetric buckling can be obtained by either substituting $\tan\theta = \theta$,

$\theta = 1.4303\pi$ and $\gamma = 1$ into Eq.(105) or $\theta = 1.4303\pi$ into Eq.(I-4) to (I-6) in Appendix I. The solutions are real when $\lambda_{ant} \geq 17.40$.

The symmetric bucked shape can be obtained by setting Eq. (96) equals to zero, gives

$$\tan\theta = \frac{-2\theta}{\beta_\theta} \tag{106}$$

The solution of transcendental equation (106) can be written as

$$\theta_{sym} = n_{sym}\pi \tag{107}$$

where n_{sym} is a constant. Therefore, the symmetric buckling mode shape may be calculated by substituting Eq. (106) into four linear algebraic Eq. (94), giving

$$v_{bsym} = G_4[\cos(\mu z) - \cos\theta] \tag{108}$$

Using Eq. (33), the corresponding axial compressive force is

$$N_{sym} = \frac{\mu^2 EI_x}{(L/2)^2} = \frac{(n_{sym}\pi)EI_x}{(L/2)^2} \tag{109}$$

It can be seen from Eq. (106) when $\beta_\theta = 0$ (pin-supported arches), $\tan\theta = \infty$, therefore $\theta = \frac{\pi}{2}$.For fixed-supported arches $\beta_\theta = \infty$ and $\theta = \pi$.

Hence, as rotational stiffness varies from 0 to infinite, n_{sym} has a range of:

$$\frac{1}{2} \leq n_{sym} \leq 1 \tag{110}$$

If one substituting $\tan\theta = \infty$, $\theta = \frac{\pi}{2}$ and $\gamma = \frac{1}{2}$ into Eq. (105) (pin-supported arches), it yields $\lambda_{sym} = 3.88$, while substituting $\tan\theta = 0$, $\theta = \pi$ and $\gamma = \infty$ gives $\lambda_{sym} = 7.69$.

These values of λ_{sym} defines the smallest modified slenderness ratio that permits any kind of buckling. Therefore, one may conclude when $\lambda < \lambda_{sym}$, in-plane buckling will not occur.

4.3 SNAP-THROUGH BUCKLING

In addition to bifurcation buckling, an elastically supported arch may also buckle in a snap-through mode. This mode is characterized by a sudden visible jump from an equilibrium state to another equilibrium state where displacements are larger than those of the prebuckling state. In this circumstance, axial compressive force in the buckled configuration N^* is different from N in the prebuckling configuration, therefore, membrane strain ε_{mb} during buckling does not vanish.

For symmetric snap-through buckling of an arch, the buckling displacement v_b is symmetric. Substituting Eq. (48) into (86) leads to the buckling differential equilibrium equation for the symmetric buckling of a shallow arch as

$$v_b^{IV} + (\mu^*)^2 (v_b)'' = \frac{\varepsilon_{mb}}{r_x^2 p}[1 + \omega(1 - \frac{\gamma \cos(\mu z)}{\cos\theta})] \tag{111}$$

The solution to Eq. (111), must satisfies the boundary conditions $v_b = 0$ at $z = \pm L/2$ and

$$[EI_x (v_b)'' + k_\theta (v_b)']_{z=L/2} = 0 \tag{112}$$

$$[EI_x (v_b)'' - k_\theta (v_b)']_{z=-L/2} = 0 \tag{113}$$

Integrating Eq. (111) twice gives

$$v_b'' + (\mu^*)^2 v_b = \frac{\varepsilon_{mb}(\omega+1)}{2r_x^2 p} z^2 + \frac{\varepsilon_{mb}\gamma\omega}{r_x^2 p \mu^2 \cos\theta} + F_1 z + F_2 \tag{114}$$

For the sake of simplicity, asterisk may be disregarded.

The solution to this second order differential equation is the sum of a homogenous and a particular solution in the following form

$$v_{\mathrm{H}} = C\cos(\mu z) + D\sin(\mu z) \tag{115}$$

$$v_{\mathrm{P}} = F_3 z^2 + F_4 z + F_5 + F_6 z \sin(\mu z) \tag{116}$$

Substituting v_p and (v_p'') into Eq. (114) gives the coefficients F_3, F_4, F_5 and F_6 in terms of F_1 and F_2.

Therefore, the general solution to Eq. (114) becomes

$$v_b = C\cos(\mu z) + D\sin(\mu z) + \frac{\varepsilon_{mb}(\omega+1)}{2r_x^2 p} z^2 + \frac{F_1}{\mu^2} z + \frac{F_2}{\mu^2} - \frac{\varepsilon_{mb}(\omega+1)}{r_x^2 \mu^4 p} + \frac{\varepsilon_{mb}\omega\gamma}{2r_x^2 \mu^3 p} z\sin(\mu z) \qquad (117)$$

Coefficients C, D, F_1 and F_2 in Eq. (117) are calculated using boundary conditions $v = 0$ at $z = \pm\frac{L}{2}$ and Eqs. (112) and (113).

These coefficients are calculated and are

$$C = \frac{\varepsilon_{mb}}{r_x^2 \mu^2 p\,(2\mu^2\cos\theta + \frac{2\beta_\theta \mu \sin\theta}{L})}[(\omega+1)(\beta_\theta+2) - \gamma\omega\theta\tan\theta + \gamma\omega(2+\frac{\beta_\theta}{2}) + \frac{\gamma\omega\beta_\theta\tan\theta}{2\theta}] \qquad (118)$$

$$D = 0 \qquad (119)$$

$$F_1 = 0 \qquad (120)$$

$$F_2 = \frac{\varepsilon_{mb}}{r_x^2 \mu^2 p}[\omega + 1 - \frac{\gamma\omega\theta\tan\theta}{2} - \frac{(\omega+1)\theta^2}{2}]$$

$$- \frac{\varepsilon_{mb}}{r_x^2 \mu^2 p(2+\frac{\beta_\theta\tan\theta}{\theta})}[(\omega+1)(\beta_\theta+2) - \gamma\omega\theta\tan\theta + \gamma\omega(2+\frac{\beta_\theta}{2}) + \frac{\gamma\omega\beta_\theta\tan\theta}{2\theta}] \qquad (121)$$

Substituting Eq. (118) to (121) into Eq. (117) and rearranging, gives

$$v_b = \frac{\varepsilon_{mb}}{\mu^4 r_x^2 p}\{\frac{(1+\omega)}{2}[(\mu z)^2 - \theta^2] + \frac{\gamma\omega}{2}[\frac{(\mu z)\sin(\mu z)}{\cos\theta} - \frac{2\gamma\theta\cos(\mu z)\sin\theta}{(2+\beta_\theta)\cos^2\theta}]$$
$$+ [\frac{\gamma(2+3\omega)}{2} + \frac{\gamma^2\omega}{2}][\frac{\cos(\mu z) - \cos\theta}{\cos\theta}]\} + \frac{\gamma\omega\theta}{2}(\frac{2\gamma}{2+\beta_\theta} - 1)\tan\theta \qquad (122)$$

It is noteworthy that the buckled displacements are identical in cases where shallow arches are horizontal spring supported and pin supported. If one substitutes $\beta_\theta = 0$ and $\gamma = 1$(pin-supported arch) into Eq. (122), gives

$$v_b = \frac{\varepsilon_{mb}}{\mu^4 r_x^{\ 2} p}\{\frac{(1+\omega)}{2}[(\mu z)^2 - \theta^2] + \frac{\omega}{2}[\frac{(\mu z)\sin(\mu z)}{\cos\theta} - \frac{\theta\cos(\mu z)\sin\theta}{\cos^2\theta}] + \frac{\omega}{2}[\frac{\cos(\mu z) - \cos\theta}{\cos\theta}]\}$$

which is consistent with the solution proposed by Bradford et al. (2004 and 2007).

Therefore, it may be concluded that the buckled displacements are independent of horizontal stiffness.

The total membrane strain in the buckled configuration can be calculated by substituting $v^* = v + v_b$, $w^* = w + w_b$ into Eq. (14) as

$$\varepsilon_m^{\ *} = w' + w_b' + \frac{(v' + v_b')z}{p} + v'v_b' + \frac{1}{2}(v')^2 + \frac{1}{2}(v_b')^2 \tag{123}$$

Hence, the increment of membrane strain during symmetric snap-through buckling can be obtained by subtracting Eq. (14) from Eq. (123)

$$\varepsilon_{mb} = \varepsilon_m^{\ *} - \varepsilon_m = w_b' + \frac{v_b' z}{p} + v'v_b' \tag{124}$$

where the small second-order term $\frac{1}{2}(v_b)^2$ of the buckling deformation v_b is ignored.

Subtracting Eqs. (26) and (27) from Eqs. (75) and (76) respectively, leads to

$$EA\varepsilon_{mb} + k_z(w_b)_{L/2} = 0 \tag{125}$$

$$EA\varepsilon_{mb} - k_z(w_b)_{-L/2} = 0 \tag{126}$$

Therefore, horizontal displacements at the support after buckling are given as

$$(w_b)_{L/2} = \frac{-EA\varepsilon_{mb}}{k_z} \text{ and } (w_b)_{-L/2} = \frac{EA\varepsilon_{mb}}{k_z} \tag{127}$$

According to Eqs. (48) and (122), the second and third parts of Eq. (114) are calculated as follows

$$\frac{v_b'z}{p}=\frac{\varepsilon_{mb}}{\mu^2 r_x^{\,2} p}\{(1+\omega)z^2+\frac{\omega\gamma}{2}[\frac{z\sin(\mu z)+\mu z^2\cos(\mu z)}{\mu\cos\theta}+\frac{2\gamma\theta\sin\theta z\sin(\mu z)}{(2+\beta_\theta)\mu\cos^2\theta}]$$

$$-\frac{\gamma(2+3\omega+\gamma\omega)z\sin(\mu z)}{2\mu\cos\theta}\} \tag{128}$$

$$v_b'v'=\frac{\varepsilon_{mb}}{\mu^2 r_x^{\,2} p}\{\omega(\omega+1)z^2+\frac{\omega^2\gamma}{2}[\frac{z\sin(\mu z)+\mu z^2\cos(\mu z)}{\mu\cos\theta}+\frac{2\gamma\theta\sin\theta z\sin(\mu z)}{(2+\beta_\theta)\mu\cos^2\theta}]$$

$$-\frac{\gamma\omega(2+3\omega+\omega\gamma)z\sin(\mu z)}{2\mu\cos\theta}-\frac{\gamma\omega(\omega+1)z\sin(\mu z)}{\mu\cos\theta}+\frac{\gamma^2\omega(2+3\omega+\gamma\omega)\sin^2(\mu z)}{2\mu^2\cos^2\theta} \tag{129}$$

$$-\frac{\gamma^2\omega^2}{2}[\frac{\sin^2(\mu z)+\mu z\sin(\mu z)\cos(\mu z)}{\mu^2\cos\theta}+\frac{2\gamma\theta\sin\theta\sin^2(\mu z)}{(2+\beta_\theta)\mu^2\cos^3\theta}]\}$$

The average incremental buckling membrane strain of Eq. (124) over the arch span L is equal to the constant buckling membrane strain ε_{mb} during buckling

$$\varepsilon_{mb}=\frac{1}{L}\int_{-L/2}^{L/2}(w_b^{'}+\frac{v_b'z}{p}+v'v_b')dz \tag{130}$$

Applying Eq. (127) and integrating Eqs. (128) and (129) over the length $\left[\frac{-L}{2},\frac{L}{2}\right]$ leads to an equation between the dimensionless load ω and axial force coefficient $\theta=\frac{\mu L}{2}$ during symmetric snap-through buckling given by

$$A_2\omega^2+B_2\omega+C_2=0 \tag{131}$$

in which

$$A_2=2A_1-\frac{5\gamma^2\tan\theta}{8\theta^3}-\frac{\gamma\tan\theta}{\theta^3}-\frac{\gamma^3\tan\theta}{4\theta^3}-\frac{7\gamma^2\tan^2\theta}{8\theta^2}+\frac{\gamma^2\tan^2\theta}{(2+\beta_\theta)\theta^2}+\frac{\gamma^3\tan^2\theta}{4\theta^2}+\frac{3\gamma^2\tan^2\theta}{4\theta^2}$$

$$+\frac{\gamma^3\tan^2\theta}{2(2+\beta_\theta)\theta^2}+\frac{\gamma}{\theta^2}+\frac{5\gamma^2}{8\theta^2}+\frac{\gamma^3}{4\theta^2}+\frac{\gamma\tan\theta}{2\theta}-\frac{\gamma^2\tan\theta}{(2+\beta_\theta)\theta}-\frac{\gamma^3(\tan\theta+\tan^3\theta)}{2(2+\beta_\theta)\theta} \tag{132}$$

$$B_2 = 2A_1 + B_1 + \frac{1}{\theta^3}[\gamma\theta - \gamma\tan\theta + \frac{\gamma^2\theta}{2} - \frac{\gamma^2\tan\theta}{2} + \frac{\theta^2\gamma\tan\theta}{2} + \frac{\gamma^2\theta\tan^2\theta}{(2+\beta_\theta)} - \frac{\gamma^2\theta^2\tan\theta}{(2+\beta_\theta)}] \quad (133)$$

$$C_2 = B_1 - C_1 = -(\frac{\theta}{\lambda})^2[1 + \frac{EA}{L}\frac{2}{k_z}] + \frac{1}{\theta^2}[\gamma - \frac{\gamma\tan\theta}{\theta} + \frac{\theta^2}{3}] \quad (134)$$

For a pair of given spring stiffness values (i.e. k_z and k_θ), the corresponding limit of modified slenderness ratio λ may be calculated by equating $q_{smy}\,p = q_{ant}\,p$ at $\theta = \pi$, where π is the fundamental solution to anti-symmetric buckling.

In a simple case where supports are pin-connected (i.e. $k_z =$ infinity, $k_\theta = 0$), λ equals to 9.38, which defines a switching point of snap-through buckling modes from symmetric to anti-symmetric buckling. This value is the same as that reported by Bradford *et al.* (2004), and Pi *et al.* (2007).

For a fix-supported arches, threshold for antisymmetric buckling mode may be obtained in the same method for pin-supported arches, which gives $\lambda_{ant} = 18.60$. The Buckling load of the symmetric mode and corresponding value of λ can be obtained by solving Eq. (57) and (131) if stability parameter μ that is known.

However, in the design or stability checking process, it is the value of λ rather than μ is known for a shallow arch, which means an iteration process is required to obtain the symmetric buckling load. As suggested by Bradford *et al*. (2004), an approximation solution for pin-ended support arch is given as

$$q_{sym}\,p \approx (0.15 + 0.0063\lambda^2)N_p \quad (135)$$

where N_p is the second mode buckling load of a pin-ended column: $N_p = \frac{\pi^2 EI_x}{(L/2)^2}$.

Considering Eq. (48), the central vertical displacement v_c at the crown of the arch is

$$v_c = \frac{\omega}{\mu^2 p}[\gamma(\sec\theta - 1) - \frac{\theta^2}{2}] \tag{136}$$

where ω can be found by solving the quadratic Eq. (131) as $\omega = \frac{-B_2 \pm \sqrt{B_2^2 - 4A_2C_2}}{2A_2}$.

Substituting ω into Eq. (136) and calculating the limit of v_c when $\theta = \frac{\pi}{2}$(since $\frac{\pi}{2}$ is the fundamental solution to symmetric buckling) leads to:

$$\lim_{\theta \to \frac{\pi}{2}} v_c = \frac{(\beta_\theta + 4)L^2}{\pi^3 p}(1 \pm \sqrt{1 - \frac{\pi^6(1+\alpha)}{64\lambda^2}}) \tag{137}$$

It's easy to show from Eq. (137) that if the arch is pin-supported, vertical displacement at the crown is real only when $\lambda \geq 3.88$; while when λ is below this limit, buckling of the shallow arch doesn't occur.

The hierarchy of buckling modes associated with different support conditions are summarized in the Table 2.

Table 2. Summary of buckling modes for various arches

Buckling mode	Pin-supported arches	Fix-supported arches	Horizontally restrained arches($k_\theta = 0$)	Rotationally restrained arches($k_z = 0$)
No buckle likely	$\lambda < 3.88$	$\lambda < 7.69$	$\lambda < 3.88\sqrt{1+\alpha}$	Buckling modes depend on stiffness ratio (β_θ).
Symmetric buckling	$3.88 \le \lambda < 7.38$	$7.69 \le \lambda < 17.40$	$3.88\sqrt{1+\alpha} \le \lambda < 7.38\sqrt{1+\alpha}$	
Sym. or antisym. buckling	$7.38 \le \lambda < 9.38$	$17.40 \le \lambda < 18.60$	$7.38\sqrt{1+\alpha} \le \lambda < 9.38\sqrt{1+\alpha}$	
Antisymmetric buckling	$\lambda \ge 9.38$	$\lambda \ge 18.60$	$\lambda \ge 9.38\sqrt{1+\alpha}$	
	Note: $\lambda = 2f / r_x$, $\beta_\theta = k_\theta L / EI_x$ and $\alpha = EA / k_z L$			

The modified slenderness ratio of an arch is an important parameter that governs the non-linear behavior of the arch. When modified slenderness ratio λ becomes sufficiently small (as indicated in the second row), the shallow arch will not snap-through and its behavior is similar to a beam curved in elevation (Pi et al. 2008).

5 .0 EFFECTS OF HORIZONTAL SPRINGS ON BUCKLING LOAD

The effects of the stiffness of horizontal restraints are analyzed in the case where rotational flexibilities are zero. By setting $\beta_\theta = 0$ and $\gamma = 1$ in Eqs. (57) and (131), the corresponding thresholds of modified slenderness ratio λ are obtained as the following

(1) when $\lambda < 3.88\sqrt{1+2\alpha}$, the buckling of the shallow arch doesn't occur;

(2) when $3.88\sqrt{1+2\alpha} \le \lambda < 7.83\sqrt{1+2\alpha}$, only symmetric buckling is possible;

(3) when $7.83\sqrt{1+2\alpha} \le \lambda < 9.38\sqrt{1+2\alpha}$, either symmetric or anti-symmetric buckling may occur;

(4) when $\lambda \ge 9.38\sqrt{1+2\alpha}$, only anti-symmetric buckling is possible.

Therefore, the thresholds of different buckling modes are amplified by the coefficient $\sqrt{1+2\alpha}$ compared to the pin-supported arches. For arches with the same modified slenderness ratio, horizontally spring-supported arches are more likely to buckle in a symmetric mode or just simply stay unbuckled.

Substituting $\beta_\theta = 0$ and $\gamma = 1$ into Eq. (105) for horizontally spring-supported shallow arches and varying parameters α and λ from 0 to 8 and 8 to 110, respectively, gives Figure 3. Figure 3 displays the variation of dimensionless buckling load qp/N verses modified slenderness ratio λ at the stiffness ratio $\alpha = 0, 2, 4$ and 8. This shows the buckling load approaches 1 as λ increases i.e. as f increases, see Eq. (61). However, the rate of increasing buckling load qp/N is

dropping as λ increases. It's noteworthy to observe that buckling loads increase rapidly when arches are shallower.

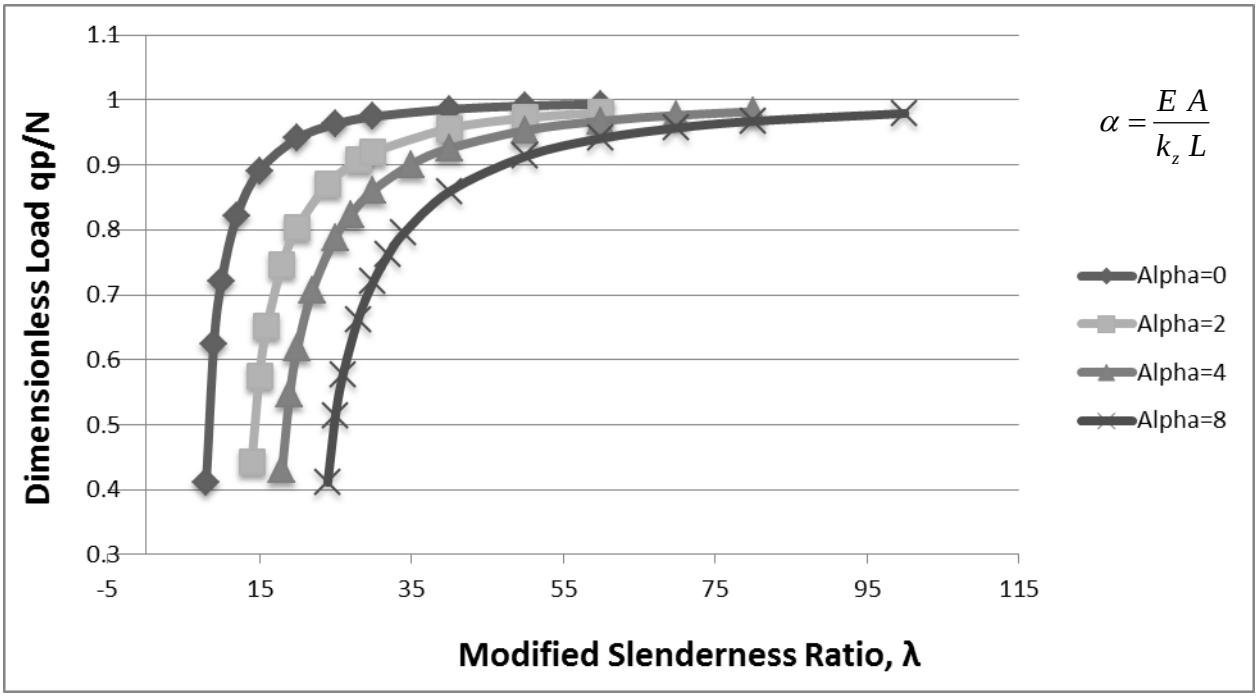

Figure 3. Buckling load for horizontally spring supported arch versus modified slenderness ratio

Figure 4 is generated using the same method as Figure 3, with horizontal axis representing the stiffness ratio α. Figure 4 illustrates the relationship between buckling load qp/N and stiffness ratio α with various modified slenderness ratios λ. It may be noted that the buckling load decrease with the increase of the stiffness ratio α (i.e. with a decrease of the horizontal stiffness k_z). It is also worth noting that buckling loads barely changes for non-shallow arches ($\lambda > 50$) with varying stiffness ratio.

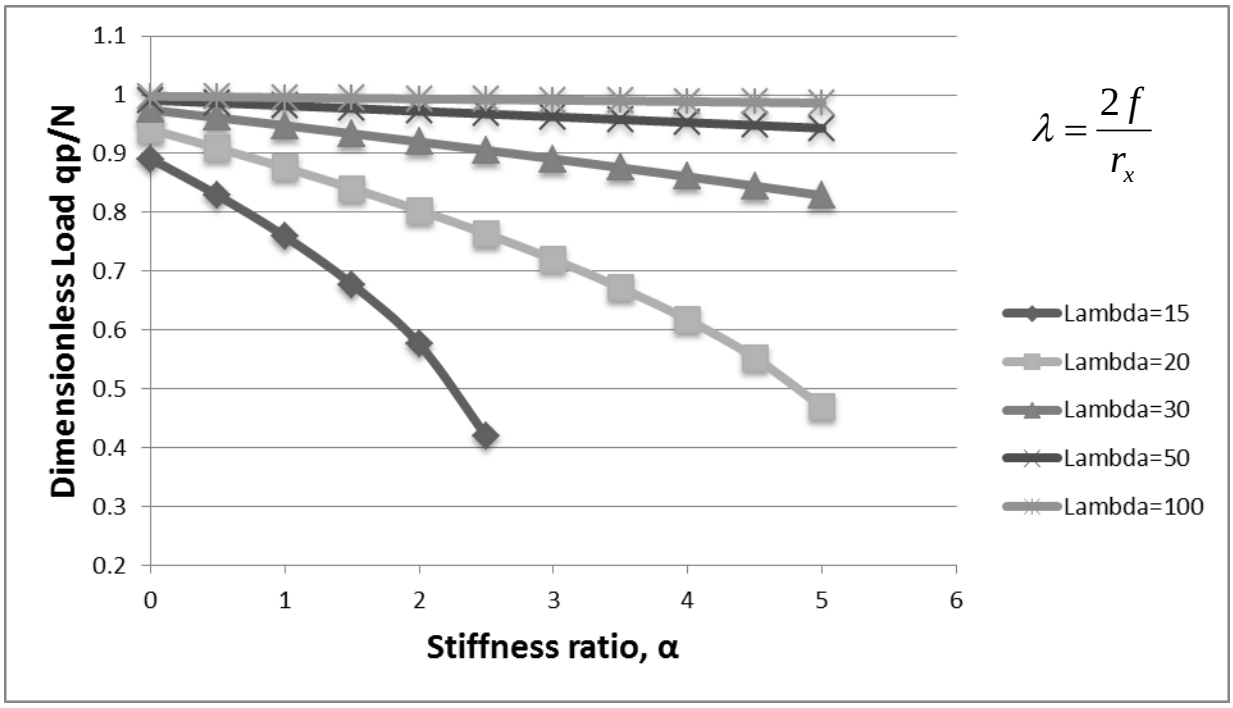

Figure 4. Effects of stiffness of horizontal restraint on buckling load

6.0 EFFECTS OF ROTATIONAL SPRINGS ON BUCKLING LOAD

Recall from Section 4.2, as stiffness of rotational spring varies from zero to infinity, n_{ant} and n_{sym} have ranges of

$1 \le n_{ant} \le 1.4303$ and $\frac{1}{2} \le n_{sym} \le 1$

For a specific value of n_{ant} in the range of 1.0 to 1.4303, the corresponding values of β_θ, γ and θ can be calculated using Eqs. (51) and (101). Substituting $\beta_\theta, \gamma, \theta$ and $\alpha = 0$ into Eq. (105) gives Figure 5 which describes the nonlinear relationships between the constant n_{ant} and dimensionless buckling load qp/N, and consequently between qp/N and rotational stiffness k_θ.

Figure 5 shows that buckling load decrease with the increase of n_{ant} (i.e. the increase of rotational stiffness k_θ). It may be concluded that with stronger rotational springs, arches are more likely to buckle. It is also worth noting that the buckling load for shallow arches tend to decrease more rapidly compared to less shallow arches when rotational stiffness increases. This is characterized by the significance of non-linearity of the shallow arches.

When the stiffness of rotational restraint vanishes, the solution of Eq. (105) leads to buckling loads for pin-supported arches, and when the rotational stiffness becomes infinite, the solution leads to the buckling loads for fully fixed arches that have been reported in Pi et al. (2007).

For symmetric bifurcation buckling, Eq. (106) may be written in an alternative form

$$\frac{\beta_\theta \tan(\theta)}{\theta} = -2 \tag{138}$$

It is interesting to notice that when substituting Eq. (138) into Eq. (51), the coefficient γ becomes infinite and there's no real solution of Eq. (57). Therefore, symmetric mode does not exist in the bifurcation buckling.

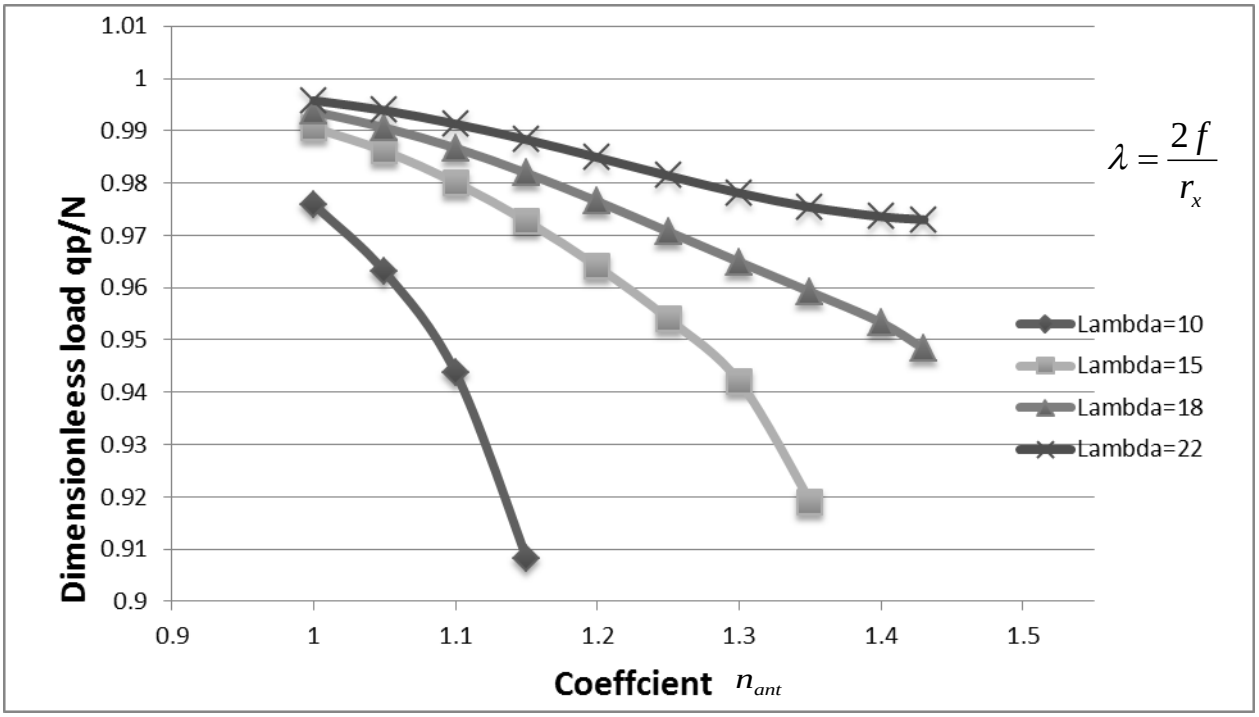

Figure 5. Effect of rotational springs on anti-s.ymmetric buckling load

7.0 EXAMPLES

In the following examples, the bahavior of shallow arches are investigated in three scenarios

(1) shallow arches that are supported by roller and horizontal springs only;

(2) shallow arches that are supported by pin and rotational springs only;

(3) shallow arches that are supported by roller, horizonal and rotational springs.

7.1 EXAMPLE 1

A shallow arch with solid rectangular section of depth $h = 45\ mm$, width $b = 400\ mm$, Young's modulus of $E = 30{,}960$ MPa and span $L = 5.1\ m$ is considered in Example 1 to 3. The data used is taken from Bradford et al. (2007), so that the results reported from their study can be compared in this thesis.

Table 3. Geometric properties for Examples

h	45 mm
b	400 mm
L	5100 mm
A	18000 mm^2
I_x	3037500 mm^4
r_x	12.99 mm

In order to study the non-linear behavior of the arch, the rise-span ratio is set to a realitively low level

$$0.01 < f/L < 0.11 \tag{140}$$

Thus, the rise f has a range of

$$51\,mm < f < 561\,mm \tag{141}$$

From Eq. (141), considering the absense of rotational springs, i.e $\beta_\theta = 0$, substituting $\beta_\theta = 0$, $\gamma = 1$, $\alpha = 0, 1.16, 1.69,$ and 3.98 into Eq. (105) , provides data for Figure 6.

Figure 6 shows the variation of dimensionless buckling load qp/N versus modified slenderness ratio λ at different stiffness ratio α without rotational springs, these data are more conservative than those obtained by Bradford et al. (2007).

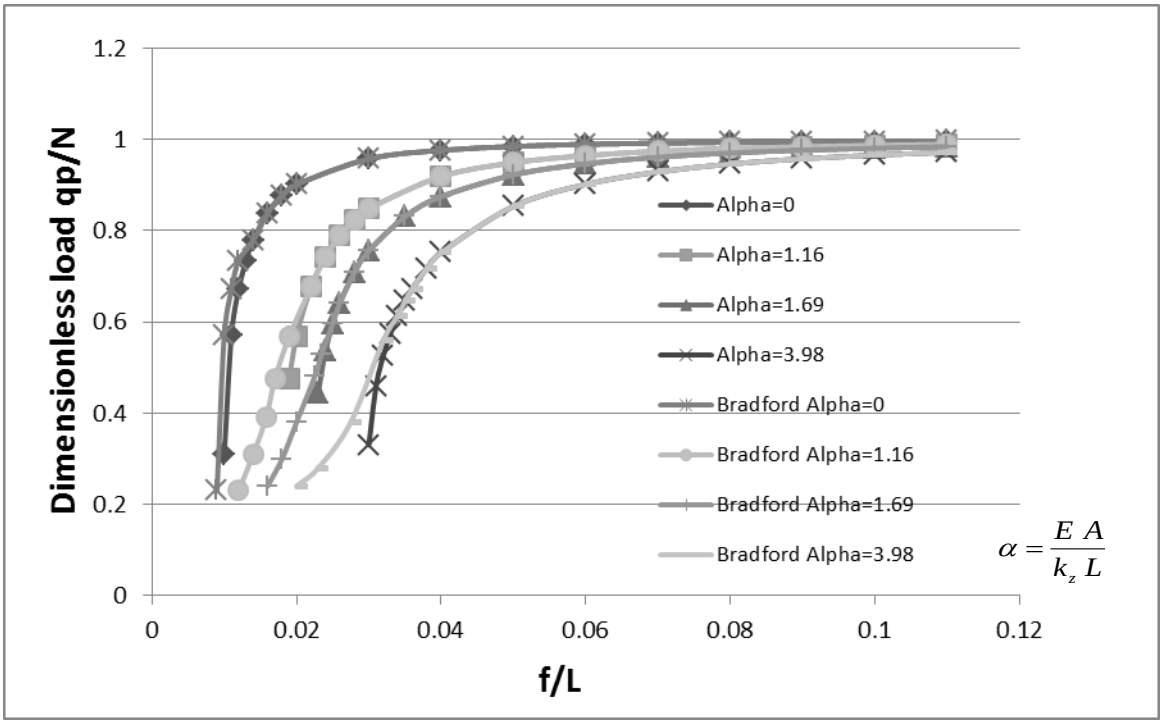

Figure 6. Buckling load versus f/L for Example 1

7.2 EXAMPLE 2

In this example shallow arches supported by pin and rotational springs are investigated. Three sets of rotational springs, which have same numerical valus as horizontal springs of Example 1 are used. Corresponding values are summerized in Table 4.

Table 4. Values of α and β_θ with respect to various spring stiffness

Set No.	Rotational Spring Stiffness(KN·mm/rad)	Horizontal Spring Stiffness(KN/mm)	α	β_θ
1	94.20	94.20	1.16	5.11
2	54.91	54.91	1.69	2.98
3	27.45	27.45	3.98	1.49

Typical variation of dimensionless buckling load versus rise-span ratio f/L at $\beta_\theta = 5.11, 2.98,$ and 1.49 are showed in Figure 7.

Figure 7 shows that buckling load almost tripled in very shallow arches ($f/L \le 0.02$) compared to Example 1. Therefore it is reasonable to conclude that rotational springs are more efficient in increasing buckling load compared to horizontal springs.

It is also noteworthy that buckling loads qp/N suffer less fluctuations even if stiffness of rotational springs are more than tripled i.e. β_θ varies from 1.49 to 5.11. Thus, the buckling load of shallow arches are more affected by horizontal springs rather than rotational springs.

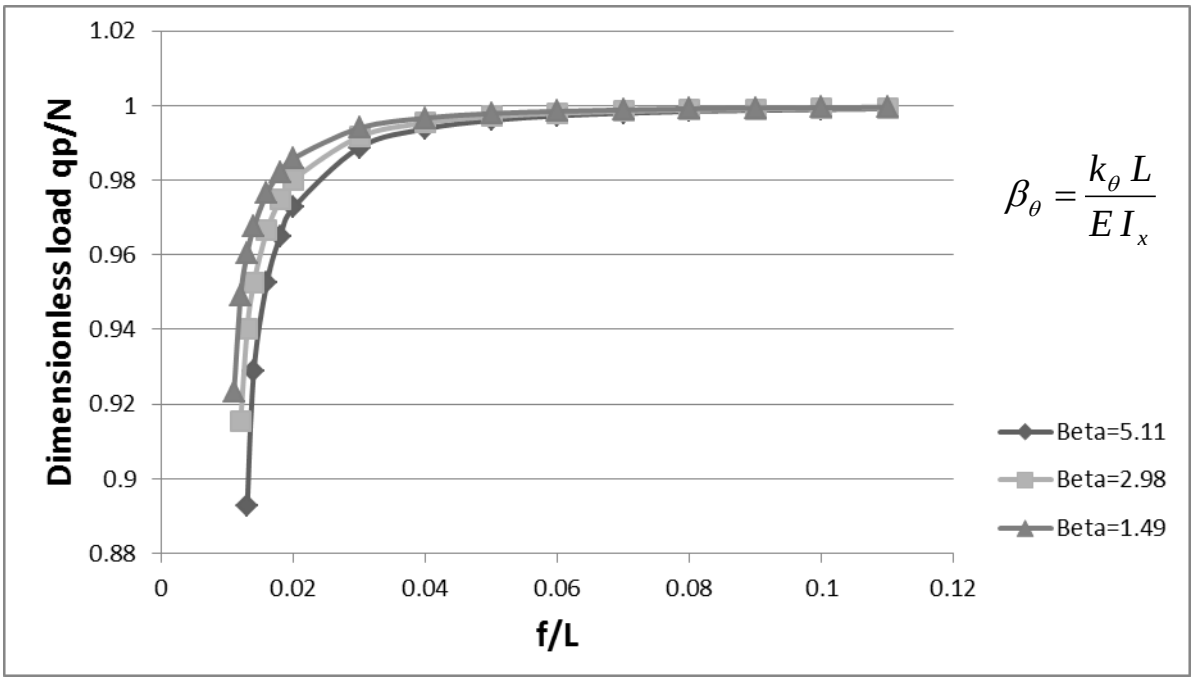

Figure 7. Buckling load versus f/L for Example 2

7.3 EXAMPLE 3

shallow arches supported by roller, horizontal and rotational springs are studied in Example 3.

In this example, the combination of springs falls into 3 cases where stiffness of horizontal and rotational springs are numerically identical, see Table 3. Substituting the values of α and β_θ from Table 3 and their corresponding values of $\gamma, \theta,$ and $\tan\theta$ into Eq. (105) gives Figure 8, which demonstrates the relationship between demensionless load qp/N and rise-span ratio f/L.

Figure 8 shows that buckling load for case 1 and case 2 are almost coincided with each other, while case 3 is a few distance away. It may be inferred from

Figure 8 that buckling load are more affected by horizontal springs instead of rotation springs. Since buckling load remain almost the same as β_θ decrease for half in case 1 and 2 from 5.11 to 2.98, while the buckling load decreases with the increase of stiffness ratio α for case 3.

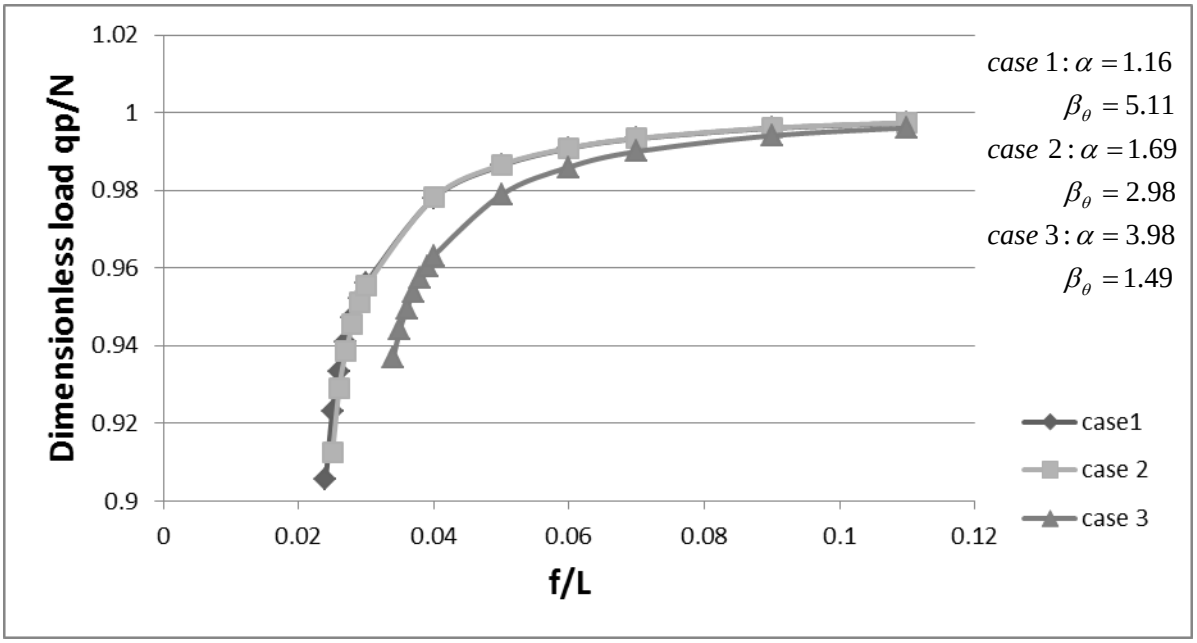

Figure 8. Buckling load versus f/L for Example 3

7.4 EXAMPLE 4

Equation of equilibrium for shallow arches with flexible support that are defined by k_z and k_θ is derived in Chapter 3 and is given by Eq. (57). Coefficients A_1, B_1, and C_1 are defined by Eqs. (58) to (60). If supports of the arch are pin connected,

the general form of the Eq. (57) remains the same, however, coefficients A_1 to C_1 will be simplified and are given by Eqs. (66) to (68) in Chapter 3.

Steel Construction Manual of the American Institute of Steel Construction is extensively used in the design of steel structures (AISC, 2011). Experience indicates vast majority of design equations in this manual are stability based equations. If one follows the same premise, stability equations derived in this thesis may be suitable for design of shallow arches.

To avoid long and tidies design process, starting from scratch, an existing shallow bridge that was designed in metric systems in Croatia is redesigned in US customary system in this example. First, a few words about the bridge itself is desirable.

Skradin Bridge in Croatia

The old Skradin Bridge was a two lanes, two hinged steel truss bridge located over the Krka River in Croatia. The bridge was destroyed during the World War II. A new bridge was constructed after the War that was opened to traffic in 1955. It is reported that most of the usable parts of the old bridge are used in the construction of the new bridge (Savor et al. 2010). The new bridge comprises of two shallow steel arch ribs spaced at 5 m apart. The span length of the bridge is 90 m. The arch ribs are hollow rectangular sections that are filled with concrete. The elevation of the bridge is shown in Figure 9. Dimensions of a typical cross section of the bridge are shown in Figure 10. The rise span ratio of this arch bridge is 7.73/90.0 = 0.0859 that satisfies the requirement of $0.01 < f/L < 0.11$ to be considered a shallow arch bridge.

In this example the cross section of the new Skradin shallow arch is redesigned considering the bridge has hinge supports. The following data is used to estimate the live and dead load of the bridge. A uniform distributed live load of q_{live} = 0.64 kips/ft per lane that is consistent with AASHTO specification is used in all iterations. The dead load of the deck is considered to be constant and is equal to the cross section area of the deck multiply by specific weight of the reinforced concrete. q_{deck} =(0.150 kips/ft^3)(24.14 ft^2) = 3.621 kips/ft. The dimensions of the existing arch rib are used to calculate the dead load of the arch rib for the first iteration. It is assumed the arch rib is a hollow steel box with the outer dimensions of 41 by 32 inches. The thickness of the arch rib is considered to be 1 inch. See Figure 11 for rib detail. The dead load of the steel tub is

$$q_{steel\ tub} = 0.489 \times [(2 \times 32 \times 1 + 2 \times 39 \times 1)/144] = .482 \text{ kips/ft} \quad (142)$$

where specific weight of steel is 0.489 kips/ft^3. Concert filled in arch rib is considered to be high strength concrete with strength limit of f_c' = 8000 psi.

According to AASHTO Specifications, specific weight of high strength concert may be calculated from

$$\gamma_{con} = 0.140 + 0.001 f_c' \text{ kips/ft}^3 \quad \text{for} \quad 5.0 \le f_c' \le 15.0 \text{ ksi} \quad (143)$$

Therefore, $\gamma_{con} = 0.148$ kips/ft^3 and the dead weight of concert is

$$q_{con} = 0.148 \times [(30 \times 39)/144] = 1.203 \text{ kips/ft} \quad (144)$$

The dead weight of the arch is the sum of these two items

$$q_{arch} = q_{steel\ tub} + q_{con} \quad (145)$$

$$q_{arch} = 1.685 \text{ kips/ft}$$

The dead weight of the bridge is the sum of the dead weight of the deck and the arch

$$q_{weight} = 3.621+1.685 = 5.306 \text{ kips/ft} \quad (146)$$

There are also railing and columns between the deck and the two arches and other accessories that are not included here. In order to account for all dead loads 15% is added to calculated dead weight. Factor dead load based on AASHTO

Specifications considering strength type I is

$$q_{factor} = 1.25\,DC + 1.5\,DW + 1.75\,(1+0.33)\,LL \quad (147)$$

$$q_{factor} = 1.25 \times 5.306 + 1.5 \times 15\% \times 5.306 + 1.75 \times 1.33 \times (2 \times 0.64) = 10.806 \text{ kip/ft}$$

Modulus of elasticity of normal strength steel is well defined and $E_s =$ 29000 ksi is used in this example. American Concert Institute (ACI) provides the following equation to calculate modulus elasticity of the concert (ACI 318-11)

$$E_c = 40000\sqrt{f_c'} + 1.0 \times 10^6 \text{ psi} \quad (148)$$

The modulus of elasticity of 8000 psi high strength concert is $E_c = 4580$ ksi. The ratio of the modulus elasticity of the steel to concert is $n = 6.33.$

Moment of inertia and cross section area of this composite section is calculated. They are $I_x = 745921.61$ in4 and $A = 4137.72$ in^2, respectively. The radius of gyration of the cross section is $r_x = 13.427$ in.

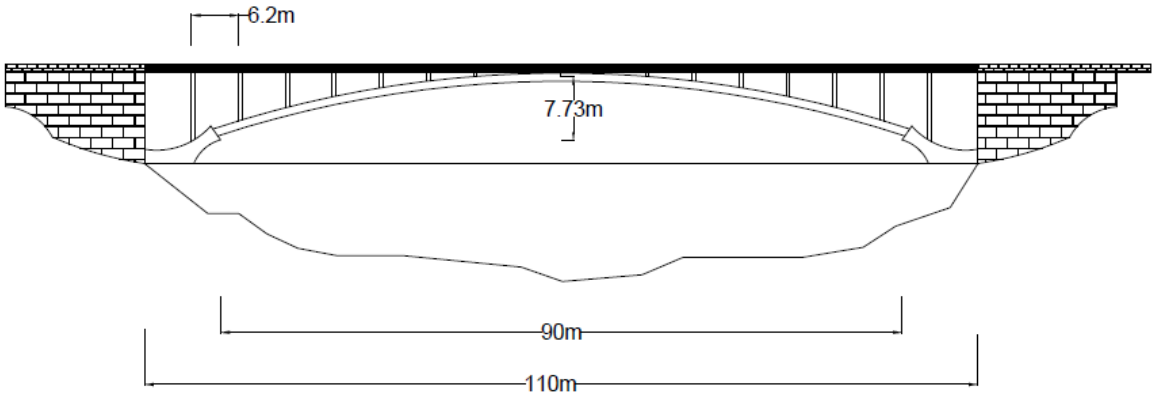

Figure 9. Longitudinal section of Skradin Bridge

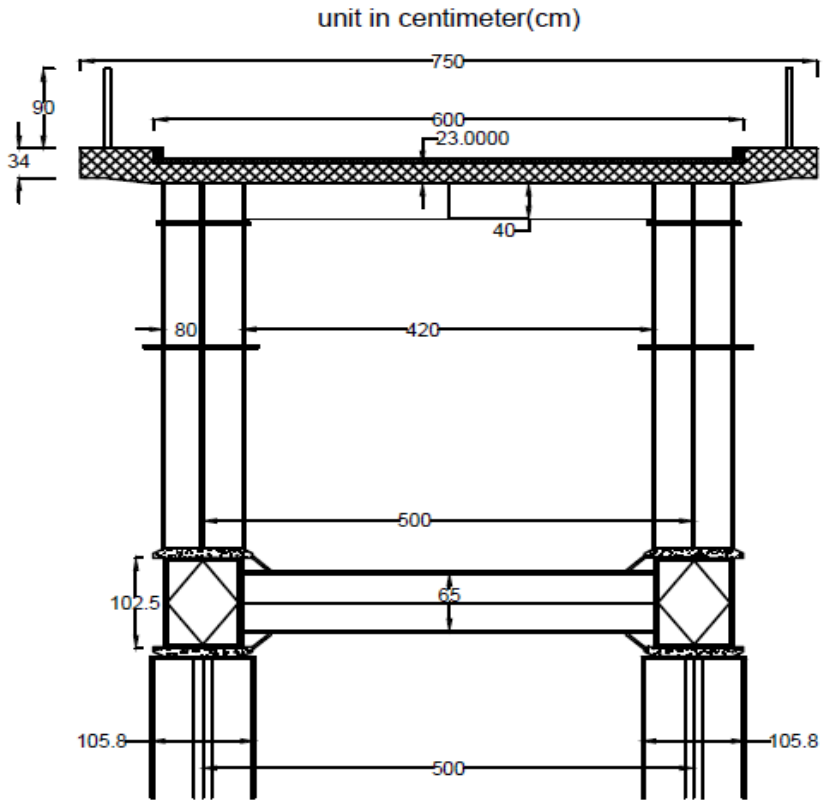

Figure 10. Typical cross section of Skradin Bridge

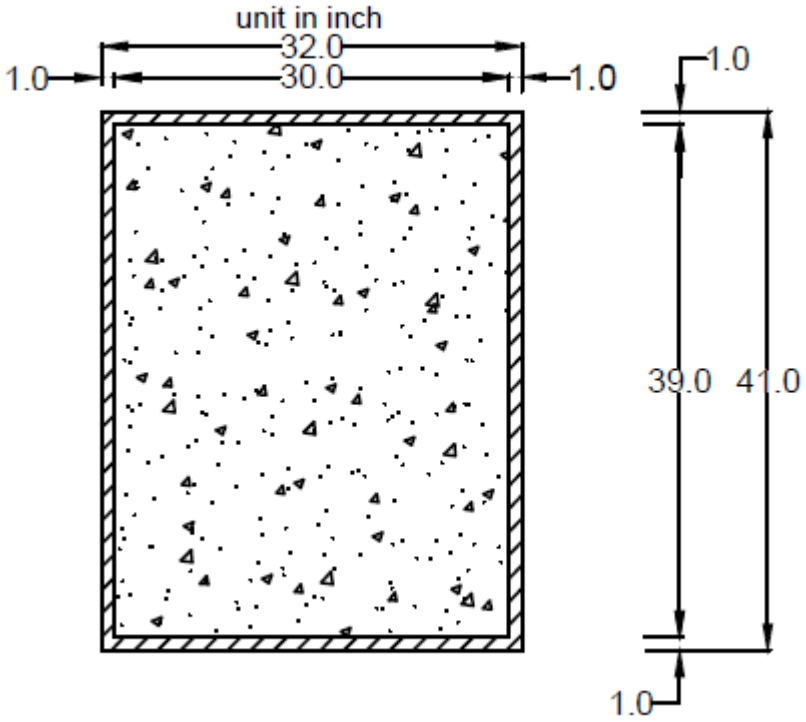

Figure 11. Rib detail for 32×41inches cross section

7.4.1 Calculation of provided distributed load

Dimensionless load ω may be calculated from Eq. (57)

$$\omega = -\frac{B_1}{2A_1} \pm \sqrt{\left(\frac{B_1}{2A_1}\right)^2 - \frac{C_1}{A_1}} \tag{149}$$

On the other hand, dimensionless load ω is defined in Eq. (34)

$$\omega = \frac{qp - N}{N} \tag{150}$$

Eliminate ω between these two equations

$$q = \frac{1}{p}\left[1 - \frac{B_1}{2A_1} \pm \sqrt{\left(\frac{B_1}{2A_1}\right)^2 - \frac{C_1}{A_1}}\right] N \tag{151}$$

From Eq. (2)

$$p = \frac{L^2}{8f} \tag{152}$$

where, L = 90 m = 295.276 ft = 3543.307 in. and f = 7.73 m = 25.361 ft = 304.331 in.

For pin-pin supported shallow arch as discussed in Section 4.2 , for anti-symmetric mode $\theta = \pi$, $\lambda \geq 7.829$, and $N = N_p$

$$A_1 = 0.2933$$

$$B_1 = 0.4347$$

$$C_1 = \frac{\pi^2}{\lambda^2} \tag{153}$$

$$N_p = \frac{\pi^2 E I_x}{(L/2)^2}$$

Substitute these data in Eq. (151) and calculate buckling distributed load $q = 24.7138$ kips/ft. Then,

$$q_{provided} = \varphi\, q_{buckling} \tag{154}$$

$$q_{provided} = 0.9 \times 24.7138 = 22.242 \text{ kips/ft}$$

and since

$$q_{factor} = q_{required} = 10.806 \ kips/\ ft < q_{provided} = 22.242 \ kips/\ ft \tag{155}$$

With the existence of relative horizontal drift and rotational movements, the provided load may be dropped to a reasonable level, and therefore, the original design achieved a safe yet economy design.

8.0 SUMMARY AND CONCLUSIONS

In this thesis, a non-linear stability analysis of shallow parabolic arches with elastic restraints subjected to a vertically uniform distributed load is investigated. An in-plane strian is first established by use of Lagrangian expression. Equilibrium conditions are then derived by total potential energy equations. A non-linear buckling analysis is then undertaken that delineates the buckling mode, and provides accurate solutions for symmetric and anti-symmetric buckling of shallow arches with horizontal and rotational spring supports.

Several findings are listed below

- It is found that the effects of stiffness of horizontal and rotational springs on the buckling load of the arch, and on the classification of different types of fundamental behavior, are significant.
- It is also found buckled displacements are irrelevant to stiffness ratio α.
- Whether or not an arch may buckle is found to depend on the modified slenderness ratio of the arch and on the stiffness of the elastic restraints, and this relationship is derived in this thesis.
- An arch with sufficiently small modified slenderness ratio will not buckle, and it will behave as a beam curved in elevation.
- It is also found that rotational springs are more effective in increasing buckling load.

9.0 FUTURE WORK

Future efforts should be implemented with the following focuses

- Carrying out finite element verifications on the buckling load of aches with various modified slenderness ratio and stiffness of elastic restraints.
- Calculation of the numerical solution for symmetric snap-through buckling load of arches with both horizontal and rotational springs for design and stability analysis purposes.
- Discussion on the more complicated external load, i.e. radial load distributed around arch axis, or uniform distributed load plus a central concentrated load.

APPENDIX

NON-LINEAR EQUILIBRIUM CONDITION FOR FIXED ARCH

Similar to the work presented in this thesis, the vertical displacement v for fixed supported arches, which satisfy the boundary conditions $v = v' = 0$ at $z = \pm\frac{L}{2}$ can be obtained by solving differential equation (18) as

$$v = \frac{\omega L \cos(\mu z)}{2\mu p \cos\theta} + \frac{\omega z^2}{2p} - \frac{\omega L}{2\mu p \tan\theta} - \frac{\omega L^2}{8p} \tag{I-1}$$

Since horizontal displacement is prevented in the fixed supported arches,

$$w_{\pm L/2} = 0 \tag{I-2}$$

Consider Eq. (55), (I-2), and substitute Eq. (I-1) into Eq. (54) leads to nonlinear equilibrium condition for fixed arches as

$$A_3\omega^2 + B_3\omega + C_3 = 0 \tag{I-3}$$

where the coefficients are given by:

$$A_3 = \frac{1}{4\sin^2\theta} - \frac{1}{4\theta\tan\theta} - \frac{1}{\theta^2}\left(1 - \frac{\theta}{\tan\theta}\right) + \frac{1}{6} \tag{I-4}$$

$$B_3 = \frac{1}{3} - \frac{1}{\theta^2}\left(1 - \frac{\theta}{\tan\theta}\right) \tag{I-5}$$

$$C_3 = \left(\frac{\theta}{\lambda}\right)^2 \tag{I-6}$$

BIBLIOGRAPHY

AASHTO LRFD Bridge Design Specifications. 2007. Customary US Units. 4th edition.

ACI 318-11. Building code requirements for structural concrete and commentary. ACI Manual of Concrete Practice, American Concrete Institute, Farmington Hills, MI.

AISC Steel Construction Manual. 14th Edition.

Austin, W. J., 1971. In-plane bending and buckling of arches. Journal of the Structural Division. ST5,1575-1592

Bradford, M.A, Pi, Y-L, Tin-Loi, F., 2002. In-plane stability of arches under a central concentrated load. J. Eng. Mech. ASCE 128(7):710-719

Bradford, M.A., Pi, Y-L., Gilbert, R.I., 2004. Nonlinear analysis of shallow parabolic arches. 17th ASCE Engineering Mechanics Conference.

Bradford, M.A., Wang, T., Pi, Y-L., Gilbert, R.I., 2007. In-plane stability of parabolic arches with horizontal supports. I: Theory. J. Struct. Eng., 133(8), 1130–1137.

Cai, J., Xu, Y., Feng, J., Zhang, J., 2010. In-plane elastic buckling of shallow parabolic arches under an external load and temperature changes. J. Struct. Eng., 138(11), 1300–1309

Dickie, J.F., Broughton. P., 1971. Stability criteria for shallow arches. J. Eng. Mech. Div. ASCE (97)EM3, 951-965

Dinnik, A.N., 1955. Buckling and Torsion. USSR, 1955,160-163. Moscow.

Gjelsvik, A., Boner, S.R., 1962. Energy criterion and snap through buckling of arches. J. Eng. Mech. Div. AECS 88(EM5):87-134

Pi, Y-L., Bradford, M.A., Tin-Loi. F., 2007. Nonlinear analysis and buckling of elastically supported circular shallow arches. International Journal of Solid and Structures. 44. 2401-2425.

Pi, Y-L., Bradford, M.A., Tin-Loi, F., 2008. Non-linear in-plane buckling of rotationally restrained shallow arches under a central concentrated load. International Journal of Non-linear Mechanics 43, 1-17

Pi, Y-L, Bradford, M.A, Uy, B., 2002. In-plane stability of arches. Int. J. Solids Struct. 39(1):102-125

Power, T.L., Kyriakides, S., 1994. Localization and propagation of instability in long shallow panels under external pressure. Journal of Applied Mechanics ASME 61(4),755-763

Savor, Z., Radic, J., Hrelja, G. 2010. Steel arch bridges in Croatia-past and present. 6th International Conference on Arch Bridges.

Simitses, G.J., 1976. An Introduction to the Elastic stability, McGraw-Hill Co. Inc., New York. USA

Schreyer, H.L. and Masur, E.F., 1966. Buckling of shallow arches. Journal of Engineering Mechanics Division. 92(4),1-17.

Timoshenko, S.P. and Gere, J.M., 1961. Theory of elastic stability. McGraw Hill, New York, USA.

Torkamani, M.A.M., 1998. Transformation matrices for finite and small rotations. J. Eng.Mech.124:359-362

Torkamani, M.A.M. and Roberts, E.R., 2009. Energy equation for elastic flexural-torsional buckling analysis of plane structure. Thin-Walled Structures 47;463-473